Vol. 44, No. 2 (2022) 322-333, DOI: 10.24874/ti.1179.09.21.01

Tribology in Industry

www.tribology.rs

RESEARCH

Computer Simulation and Optimization of Elliptic Bore Journal Bearing

Sushanta Kumar Pradhan[a], Ramanuj Kumar[b], Prakash Chandra Mishra[a,*]

[a]*Department of Mechanical Engineering , Veer Surendra Sai University of Technology, Burla, India-768018*
[b]*School of Mechanical Engineering, KIIT University, Bhubaneswar, India-751024*

Keywords:

Hydrodynamic lubrication
Elliptic bore journal bearing
Newton Raphson Method
Surface roughness
Friction force
Flow-in
Optimization of performance

Corresponding author:

Prakash Chandra Mishra
E-mail: pcmishra_me@vssut.ac.in

Received: 5 September 2021
Revised: 6 November 2021
Accepted: 19 January 2022

A B S T R A C T

In this study, the computer simulation is carried out using FORTRAN to develop a theoretical model for estimating the lubrication performance of an elliptic bore journal bearing. The Analysis initially includes the hydrodynamic lubrication principle to solve non-dimensional Reynold's equation of a finite journal bearing for bearing pressure. Subsequently, the load-carrying capacity, friction force, and lubricant flow are studied for different bearing eccentricities, non-circularity, and surface roughness parameters. The model thus developed, shows a good agreement with available research work. The results predict non-circularity up to (G=1.0) promotes better load-bearing ability, while roughness index (Y=0.1), offers the highest fluid friction. The highest non-dimensional load, friction, and flow-in are found to be 31.12, 45.19, and 6.42 respectively. The optimization shows the favorable condition for low, medium, and high load, friction, and flow-in.

© 2022 Published by Faculty of Engineering

1. INTRODUCTION

Journal bearing is a hydrodynamic bearing most widely used in rotating machinery, especially deployed in internal combustion engines and gas or steam turbines. Such bearing consists of a rotating journal supported in a stationary bore of a sleeve. Due to the converging-diverging film profile and in-compressible damping offered by flowing lubricant, it develops a reactive force after the shaft achieved the desired speed. This leads to the separation of contiguous surfaces (journal and sleeve), thereby reducing the chance of wear due to metal-to-metal contact. Journal bearings are termed as bearing of infinite life, as these are operated in full fluid film condition. The minimum film thickness, in this case, is in the range of 5μm to 100μm. Many times, it is found from experience that inclusion of surface roughness and bore non-circularity is beneficial for bearing operation and performance. Further bore ellipticity/ovality is always a possibility due to manufacturing defects such as small amplitude vibration of tools or wears due to start-stop operations. Such misalignment effects are often not considered in theoretical analysis that leading to significant variation of theoretical from experimental results.

Numerical computation on journal bearing first started in the 1950s [1]. Using this technique, journal bearing parameters are mathematically computed. Mathematical expressions for film thickness and its location, hydrodynamic action force, load, friction force, and power as well as Sommerfeld number are developed with accuracy. Standard charts are constructed for reference. Pinkus [2] developed a complete set of solutions for journal bearing by combining design and operational parameters. Such investigation was helpful in the estimation of load-carrying capacity in any direction even for bearing with multiple oil holes. It helps in identifying the optimal position of load angle, where load-carrying capacity and oil flow are maximum, while power loss is minimum.

It was the concern of researchers to develop standard data for bearing design to help field engineers understand parameters' interrelationship. Reason and Narang [3] developed a computational method for faster analysis of journal bearing. Such a technique can be used for short, finite, and long journal bearing even by using a simple calculator the parameters could be estimated. But such analysis was based on approximation. Again, such a study only considers smooth and circular journal and bearing interface, which is not the reality. In microscopic observation, there is the presence of roughness in order of 1μm. Such roughness issues should be addressed in the analysis. The quantification elliptic bore is first given by Crosby [4], through which he calculated the influence of non-circularity on bearing performance parameters. But the work reported for smooth case, whereas in actual practice there appear roughness features in bearing surface. That's why the quantification of such irregularity should be included. Christensen and Tonder [5] formulated Reynold's equation for lubrication performance of journal bearing with roughness pattern on bore surface. They developed a Reynolds type equation by the aid of stochastic theory considering film thickness in bearing as a stochastic parameter.

Further to the study on rough journal bearing, Christensen and Tonder [6] investigated various roughness orientations (Longitudinal, transverse, and isotropic) on bearing performance. They tabulated load, friction, flow-in, and flow-out for various eccentricities. Similarly, Dong Zhu et al. [7] investigated the influence of roughness irregularities (pattern and orientation) on elastohydrodynamic lubrication (EHL) and mixed lubrication. Later on, it is realized that shear thinning and bore ellipticity reduce the load-bearing ability of journal bearing. Rahmani et al. [8] investigated the effect of bore ellipticity and non-Newtonian lubricant on journal bearing operational steadiness. Compared to plain circular journal bearing, an elliptic bore bearing develops less load carrying capacity and induces more coefficient of friction.

Misalignment is another important operational inconvenience, which affects the stability and performance of a journal bearing. Mishra [9] formulated a mathematical model to investigate the effect of shaft irregularity on dynamic characteristics of non-circular journal bearing, taking into consideration the heat rise and non-Newtonian rheology. Through such analysis, the geometrical irregularities like ellipticity and roughness are integrated with an operational problem such as misalignment to monitor stiffness and damping parameters through a hybrid method of solution of Reynolds and Energy equation that uses the power-law model to address non-Newtonian effect. Further to the roughness effect in journal bearing, Majumdar et al. [10] investigated a submerged journal bearing considering thermal and hydrodynamic action. They concluded that total load-bearing ability with roughness inclusion is due to heat generation and asperity contact pressure. Considering Gaussian distribution of roughness heights, they depicted relation among surface roughness, viscous, thermal, and hydrodynamic action.

Liang et al. [11] developed an analytical method using Gauss-Legendre integral formula to evaluate quasi-static properties of hydrostatic bearing. Using this method, the recess-load and lubricant flow were estimated for different eccentric positions and wrap-angle. Binu et al. [12] studied a journal bearing with two axial holes and found hydrodynamic action experimentally. They implemented two techniques like pressure measured (a) with the sensor fitted on the journal and (b) with the sensor placed outside the setup. The pressure obtained in the second method is comparable to theoretically calculated pressure with a 20% difference.

Roughness in the bearing surface is characterized as a longitudinal, transverse, and isotropic pattern. The isotropic pattern is most preferable as it holds a compromise between the lubricant flow and pressure development. Guha [13] studied a hydrodynamic rough journal bearing for steady-state performance. Incorporating FDM, he deduced the film profile of both axially and twisted misaligned shaft and bore interface. The bearing performance characteristics such as load-bearing ability, attitude angle, lubricant leakage, friction coefficient, etc. wear obtained for different roughness ranges, eccentricity, and misalignment. Rahmani et al. [14] investigated the influence of replacing solid powders with liquid lubricants. They carried out a combined numerical and experimental analysis to compare the threshold speed of instability of power lubricated journal bearing with that of oil-lubricated bearing. Power lubricated bearing found more stable.

All the literature discussed above mostly used the finite difference technique for computation. Londe and Tonder [15] carried out a numerical simulation of lubrication of rough surfaces by FEM considering pressure-only flow conditions. Here, they presented inter-relations of, pressure-roughness height, the pressure-height gradient in 3-D form, and generated it numerically using Finite Impulse Response (FIR) filters and FFT. This study is limited to a flat surface, its application to journal bearing would be more useful. Tugra et al. [16] investigated the effects of roughness constant and pattern the steady-state characteristics of journal bearings. The transverse pattern has the ability to carry more load enhances load-bearing ability and stability with surface roughness, but in the case of other orientation, the effect is minimal.

Zang et al. [17] developed a dynamic model to investigate load sharing of journal bearing used in planetary gear systems and found that it is influenced by bearing performance. Jamali and Al-Hammod [18] formulated a method to analyze misaligned journal bearing. The method includes the solution of a Reynolds equation through the finite difference method for three-dimensional misaligned geometry. The results show ultra-thinning of lubricant film thickness results in a noticeable rise in hydrodynamic pressure at the misaligned state of the journal. Kokkinidis and Nikolakopoulos [19] carried out a computer simulation of misaligned journal bearing using a neural network. They developed an artificial neural network (ANN) model to train, test, and validate performance parameters of journal bearing evaluated using the finite difference method (FDM). Jamali and Al-Hammod [20] studied the effects of cavitation and the use of non-Newtonian lubricant on the performance of journal bearing. Kuider et al. [21] developed a mathematical model of journal bearing lubricated with non-Newtonian lubricant. The Reynolds equation of polar co-ordinate is solved through the finite difference method and the non-Newtonian property of a lubricant is quantified through the Walther equation.

Grey relational optimization is a very popular and efficient optimization tool for multi-response optimization. Also, this technique utilizes the experiment result data, and the calculations are simple and easy to understand. Several studies reported this concept for multi-response optimization for bearing problems [22-23].

Kumar et al. [24,25] formulated a multi-objective optimization practice to estimate the life of cutting tools and cutting costs, by correlating tool wear and surface characteristics. Optimization has its application in emission analysis. Mishra et al. [26] investigated an SI engine emission performance with a chambered straight muffler and identified a correct combination of the gasoline-methanol blend, torque, and speed for reduction of (CO, CO_2, NO_x, and HC). Avikal et al. [27] developed a grey optimization methodology for a multi-lobe journal bearing and suggested the most influencing parameters as film and attitude angle.

Based on this wide literature review, it is realized that there is a sizeable number of works reported in the area of lobe bearing, and also there are many reported on roughness effect on journal bearing performance. The novelty of this work is to depict the performance characteristic of bearing (Either maximum or minimum, whichever is favourable) using optimal parameters. To achieve this, the procedure developed to numerically investigate the combined effect of non-circularity (Ellipticity) and isotropic roughness on bearing performance parameters and link such parametric trends with multi-objective optimization to understand the level of influence of operational parameters on performance.

2. THEORITICAL FORMULATION

2.1 Bearing geometry with elliptic bore

The difference between circular and elliptic geometry is that the radius in circular one is constant, while that of the elliptic bore has one major radius and one minor radius. Eq. (1) shows the equation of elliptic case.

The equation of an ellipse is:

$$\left(\frac{x}{a}\right)^2+\left(\frac{y}{b}\right)^2=1 \tag{1}$$

While the bore, in this case, is considered elliptic, the shaft outer surface is taken as circular. Crosby [4] and Mishra [9] assume elliptic bore and derived the conjunctional film expression as given in Eq. (2)

$$H=1+G\cos^2\theta+\in\cos\theta \tag{2}$$

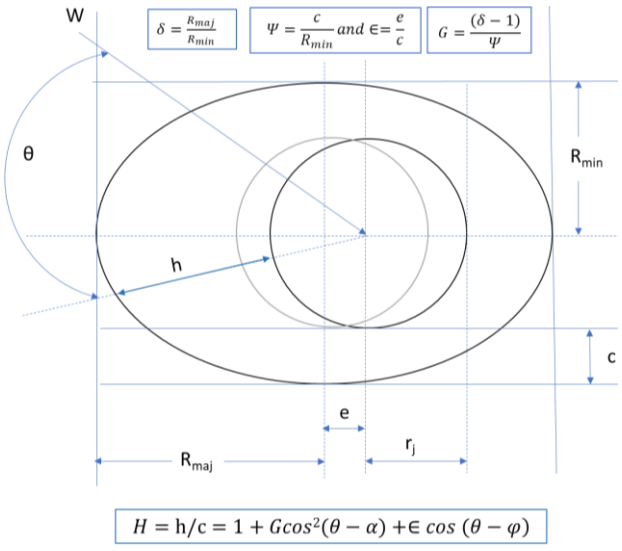

Fig. 1. Geometric model of elliptic bore journal bearing.

2.2 Governing Equation of the analysis

A lubricant film in the conjunction of journal and bearing is assumed to be regulated through Reynold's equation for an incompressible fluid which is Newtonian and iso-viscous. A modified Reynolds equation for this case is formulated in non-dimensional form. To correlate the dimensional and dimensionless variables involved in Reynold's equation as per Crosby [4] as follows:

Hence, the equation is derived to Eq. (3)

$$\frac{\partial}{\partial\theta}\left(H^3\frac{\partial P}{\partial\theta}\right)+\frac{1}{\beta^2}\frac{\partial}{\partial z}\left(H^3\frac{\partial P}{\partial Z}\right)=6\frac{\partial H}{\partial\theta} \tag{3}$$

The governing equation of a journal bearing considering roughness as per Christensen and Tonder [5] can be expressed with expectancy operators E (x) is:

$$\frac{\partial}{\partial x}\zeta\left(H^3\frac{\partial P}{\partial x}\right)+\frac{\partial}{\partial z}\zeta\left(H^3\frac{\partial P}{\partial z}\right)=6\eta u\frac{\partial}{\partial x}\zeta(H) \tag{4}$$

where

$$\zeta(x)=\int_{-\infty}^{\infty}xf(x)dx \tag{5}$$

is the Expectancy operator.

The $f(x)$ is probability density of stochastic variables. To summarize the expectancy operator Eq. (5) can otherwise be presented as per Christensen and Tonder [5] as follows:

$$\frac{\partial}{\partial x}\left(\frac{\partial P}{\partial x}\vartheta_1(H)\right)+\frac{\partial}{\partial z}\left(\frac{\partial P}{\partial z}\vartheta_2(H)\right)=6\eta u\frac{\partial}{\partial x}\vartheta_3(H) \tag{6}$$

where, modified film terms for different roughness are given in the Table1.

Table 1. Expectancy operator for different roughness structure as per Christensen and Tonder [6].

Film thickness function (Ψ_i)	Longitudinal	Transverse	Isotropic
ϑ_1	$\zeta\left(H^3\right)$	$\frac{1}{\zeta\left(\frac{1}{H^3}\right)}$	$\zeta\left(H^3\right)$
ϑ_2	$\frac{1}{\zeta\left(\frac{1}{H^3}\right)}$	$\zeta\left(H^3\right)$	$\zeta\left(H^3\right)$
ϑ_3	$\frac{1}{\zeta\left(\frac{1}{H}\right)}$	$4\zeta\left(\frac{1}{H}\right)$	$\zeta\left(\frac{1}{H}\right)$

The expression for film operators in terms of film thickness and roughness constant are tabulated in Table 2, where Y = roughness factor.

Table 2. Expectancy operator value as per [6].

Film terms	Value
$\zeta(H)$	$1+G\cos^2\theta+\in\cos\theta$
$\zeta\left(\frac{1}{H}\right)$	$\frac{35}{37Y^7}\left\{\begin{array}{l}6\left(Y^2-H^2\right)\log\left(\frac{Y+H}{Y-H}\right)\\+\frac{2}{5}YH\left(15H^4-40Y^2H^2+33Y^4\right)\end{array}\right\}$
$\zeta\left(H^3\right)$	$H^3+\frac{HY^2}{3}$

2.2.1 Pressure-Temperature-Viscosity interdependence

When there is rapid shear of the lubricant layer, the temperature in the lubricant increases due to fluid friction between adjacent layers. Such thermal change leads to degradation of the viscosity. It follows the rheological relation. There exists the interdependency among the lubricant density, film pressure, temperature rise, and the surrounding pressure. It is given in equation (7). Again, the viscosity variation with the variation of temperature and pressure is addressed using combined law by Downson and Higginson [28] given in equation (8) as

$$\rho=\rho_0\left(1-0.65\times10^{-3}\Delta\theta\right)\left[1+\frac{6\times10^{-10}\left(p-P_{atm}\right)}{1+1.7\times10^{-9}\left(p-P_{atm}\right)}\right] \tag{7}$$

$$\eta=\eta_0\exp\left\{\left(\ln\eta_0+9.67\right)\left[\left(\frac{\Theta-138}{\Theta_0-138}\right)^{-S_0}\left(1+\frac{p-P_{atm}}{1.98\times10^8}\right)^Z-1\right]\right\} \tag{8}$$

where

$$Z=\frac{\alpha_0}{5.1\times10^{-9}\left[\ln\eta_0+9.67\right]}\ and\ S_0=\frac{\beta_0\left(\Theta_0-138\right)}{\ln\eta_0+9.67} \tag{9}$$

2.3 Discretization-Convergence-Boundary conditions

The grid network for discretizing the Reynolds Eq. (3&6) is shown in Fig. 2. Expanding Eq. (3) yields:

$$3H^2\frac{\partial H}{\partial\theta}\frac{\partial P}{\partial\theta}+H^3\frac{\partial^2P}{\partial\theta^2}+\frac{1}{\beta^2}3H^2\frac{\partial H}{\partial Z}\frac{\partial P}{\partial Z}+\frac{1}{\beta^2}H^3\frac{\partial^2P}{\partial Z^2}=6\frac{\partial H}{\partial Z} \tag{10}$$

Applying central differences to the derivatives:

$$\frac{\partial^2P}{\partial\theta^2}=\frac{P_{i+1,j}-P_{i,j}+P_{i-1,j}}{\Delta\theta^2};\frac{\partial H}{\partial\theta}=\frac{H_{i+1,j}-H_{i-1,j}}{2\Delta\theta}; \tag{11}$$

$$\frac{\partial P}{\partial\theta}=\frac{P_{i+1,j}-P_{i-1,j}}{2(\Delta\theta)};\frac{\partial P}{\partial Z}=\frac{P_{i,j+1}-P_{i,j-1}}{2(\Delta Z)};\frac{\partial^2P}{\partial Z^2}=\frac{P_{i,j+1}-P_{i,j}+P_{i,j-1}}{\Delta Z^2} \tag{12}$$

And considering, $\frac{\partial H}{\partial Z}=0.$ (13)

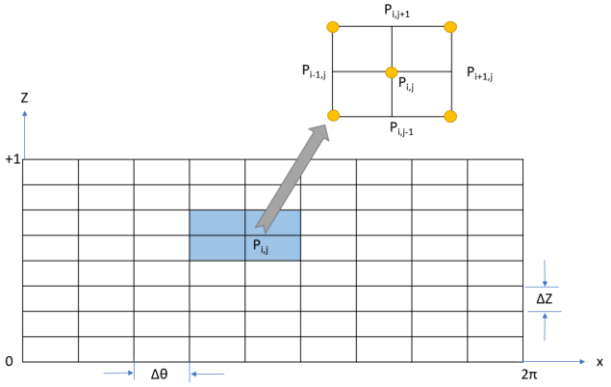

Fig. 2. Finite element mesh and grid element.

It is assumed there is no variation in film thickness in *z*-direction i.e., along bearing length. Using this discrete values, Reynolds Eq. (10) can now be written in finite difference form as:

$$\left\{\begin{array}{l}H^3\left(\frac{P_{i+1,j}-P_{i,j}+P_{i-1,j}}{\Delta\theta^2}\right)+3H^2\left(\frac{P_{i+1,j}-P_{i-1,j}}{2\Delta\theta}\right)\left(\frac{H_{i+1,j}-H_{i-1,j}}{2\Delta\theta}\right)\\+\frac{H^3}{\beta^2}\left(\frac{P_{i+1,j}-P_{i,j}+P_{i-1,j}}{\Delta Z^2}\right)=6\frac{\partial H}{\partial\theta}\end{array}\right. \tag{14}$$

Following substitutions for above Eq. (14)

$$\Upsilon_1=\frac{H_{i,j}^3}{\Delta\theta^2};\Upsilon_2=\frac{H_{i,j}^3}{\beta^2\left(\Delta Z\right)^2};\Upsilon_3=\frac{3H_{i,j}^2}{4\left(\Delta\theta\right)^2};\Upsilon_4=\frac{3}{\Delta\theta}$$

yields:

$$\Upsilon_1\left(P_{i+1,j}-2.P_{i,j}+P_{i-1,j}\right)+\Upsilon_2\left(P_{i,j+1}-2P_{i,j}+P_{i,j-1}\right)+$$
$$\Upsilon_3\left(H_{i+1,j}-H_{i-1,j}\right)\left(P_{i+1,j}-P_{i-1,j}\right)=\Upsilon_4\left(H_{i+1,j}-H_{i-1,j}\right)$$

or,

$$\Upsilon_1\left(P_{i+1,j}-2.P_{i,j}+P_{i-1,j}\right)+\Upsilon_2\left(P_{i,j+1}-2P_{i,j}+P_{i,j-1}\right)+$$
$$\Upsilon_3\left(H_{i+1,j}P_{i+1,j}-H_{i-1,j}P_{i+1,j}-H_{i+1,j}P_{i-1,j}+H_{i-1,j}P_{i-1,j}\right)=\Upsilon_4\left(H_{i+1,j}-H_{i-1,j}\right) \tag{15}$$

Rearranging Eq. (15):

$$\begin{array}{l}P_{i+1,j}\left(\Upsilon_1+\Upsilon_3H_{i+1,j}-\Upsilon_3H_{i-1,j}\right)+\\P_{i-1,j}(\Upsilon_1-\Upsilon_3H_{i+1,j}+\Upsilon_3H_{i-1,j})+\\P_{i,j+1}\Upsilon_2-P_{i,j-1}\Upsilon_2-P_{i,j}\left(2\Upsilon_1+2\Upsilon_2\right)=\Upsilon_4\left(H_{i+1,j}-H_{i-1,j}\right)\end{array} \tag{16}$$

Further substitutions in Eq. (16) are

$$\Upsilon_5 = \left(\Upsilon_1 + \Upsilon_3 H_{i+1,j} - \Upsilon_3 H_{i-1,j}\right);$$
$$\Upsilon_6 = \left(\Upsilon_1 - \Upsilon_3 H_{i+1,j} + \Upsilon_3 H_{i-1,j}\right);$$
$$\Upsilon_7 = \left(2\Upsilon_1 + 2\Upsilon_2\right);$$
$$\Upsilon_8 = \Upsilon_4\left(H_{i+1,j} - H_{i-1,j}\right).$$

Eq. (15) can be rewritten as follows:

$$\Upsilon_5 P_{i+1,j} + \Upsilon_6 P_{i-1,j} + \Upsilon_2 P_{i,j+1} + \Upsilon_2 P_{i,j-1} - \Upsilon_7 P_{i,j} = \Upsilon_8$$

$$P_{i,j} = -\frac{\Upsilon_8}{\Upsilon_7} + \frac{\Upsilon_5}{\Upsilon_7} P_{i+1,j} + \frac{\Upsilon_6}{\Upsilon_7} P_{i-1,j} + \frac{\Upsilon_2}{\Upsilon_7} P_{i,j+1} + \frac{\Upsilon_2}{\Upsilon_7} P_{i,j-1}$$

Further substitutions of

$$\Upsilon_9 = -\frac{\Upsilon_8}{\Upsilon_7}; \Upsilon_{10} = \frac{\Upsilon_5}{\Upsilon_7}; \Upsilon_{11} = \frac{\Upsilon_6}{\Upsilon_7}; \Upsilon_{12} = \frac{\Upsilon_2}{\Upsilon_7}$$

yield:

$$P_{i,j} = \Upsilon_9 + \Upsilon_{10} P_{i+1,j} + \Upsilon_{11} P_{i-1,j} + \Upsilon_{12} P_{i,j+1} + \Upsilon_{12} P_{i,j-1} \quad (17)$$

Eq. (17) provides a recursive relationship for $P_{i,j}$ at a node in terms of nodes behind and in front as well as points below and above as indicated in Fig. 2 of the developed bearing surface.

To speed up the iterative process, the over relaxation factor in case of oil lubricated bearing can be introduced as follows:

$$P_{i,j}^{K} = P_{i,j}^{K} + orf\left(P_{i,j}^{K+1} - P_{i,j}^{K}\right) \quad (18)$$

Here, '*orf*' is the over relaxation factor

The Convergence criteria adopted for pressure and temperature

$$Error = \sum_{i}^{n}\sum_{j}^{m}\left|P_{i,j}^{K+1} - P_{i,j}^{K}\right| \le 0.005 \quad (19)$$

The error tolerance of ≤ 0.0018 has been decided by trials. The convergence criteria are decreased gradually like 0.1, 0.01, 0.001, 0.0001 and the result is compared for successively decreased convergence. When result does not substantially change between two sets of convergence $P_{i,j}$ values in subsequent iterations, the higher one is adopted.

The flow chart of computation is shown in the Fig. 3 of the program developed. The recursive relation (as per Eq. 21) is used by first initializing the pressures at all nodes to be zero. This automatically satisfies the boundary conditions on the left, top and bottom sides i.e., at $\theta = 0$, $Z = 0 \& 1$. The value of $P_{i,j}$ is found by starting with $P_{1,1}$ and either moving zigzag to right hand corner node within the boundary or by moving vertically and zig-zaggers to the corner to satisfy the boundary conditions. The $P_{i,j}$ is never allowed to become negative by setting any negative value to zero. The process of iteration is stopped by checking the pressure values at all the nodes in two subsequent iterations by satisfying Eq. (13).

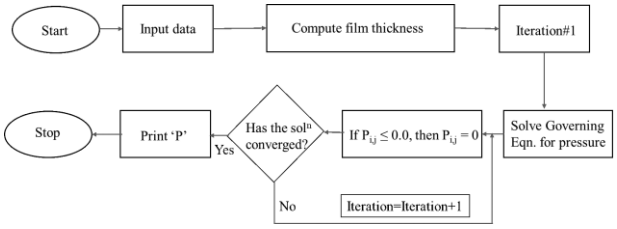

Fig. 3. Flow chart for pressure computation.

2.4 Load bearing ability of Elliptic bore bearing

The load carrying capacity of elliptic bore bearing in this case can be evaluated using Simpson rule, which is as follows:

$$W^* = \frac{\Delta\theta\Delta z}{9}\int_{\theta_0}^{\theta_m}\int_{z_0}^{z_n} P(\theta, z)\,\partial\theta\partial z$$

or

$$W^* = \frac{\Delta\theta\Delta z}{9}\left[\begin{pmatrix} P_{0,0} + 4.P_{1,0} + 2.P_{2,0} \\ +\ldots\ldots + P_{m,0} \end{pmatrix} + 4\begin{pmatrix} P_{0,1} + 4.P_{1,1} + 2.P_{2,1} \\ +\ldots\ldots + P_{m,1} \end{pmatrix} + 2\begin{pmatrix} P_{0,2} + 4.P_{1,2} + \\ \ldots\ldots + P_{m,2} \end{pmatrix} + \ldots\ldots\ldots\ldots + \begin{pmatrix} P_{0,n} + 4.P_{1,n} + 2.P_{2,n} \\ +\ldots\ldots + P_{m,n} \end{pmatrix}\right] + E \quad (20)$$

where

$$E = -\frac{\partial\theta\partial z}{9}\left[m\Delta\theta^4\frac{\partial^4 P(\xi,\eta)}{\partial\theta^4} + n\Delta z^4\frac{\partial^4 P(\xi,\eta)}{\partial^4 z}\right]$$

Implementing this rule as per Eq. (20), the non-dimensional load is estimated.

2.5 Friction force of elliptic bore bearing

The shear stress expression for rough bearing is as:

$$\tau = \frac{\eta U}{h} - \frac{h}{2}\frac{\partial p}{\partial x}$$

The friction force can be evaluated through double integration of shear stress over the contact area and is:

$$F = \int\int \tau dxdy \tag{21}$$

2.6 Flow parameters of elliptic bore bearing

The rate of flow of the lubricant is found out by using equation (22).

$$q_{in} = \frac{Uh}{2} - \left(\frac{h}{2}\right)\frac{\partial p}{\partial x} \tag{22}$$

and

$$Q_{in} = \int\int q_{in} dxdy \tag{23}$$

The rate of side leakage of the lubricant is found out by using equation (24).

$$q_s = -\left(\frac{h^2}{2}\right)\frac{\partial p_h}{\partial z} \tag{24}$$

and

$$Q_s = \int\int q_s dxdy \tag{25}$$

2.7 Optimization of performance

In this analysis, a Grey relational optimization concept is used to estimate the optimal set of journal bearing input variables to get the optimal outputs. Through this method, the equivalence is drawn between the reference sequence and compatibility sequence to depict quality characteristics. In order to achieve this, it is required to convert multi-response optimization problems to single response problems by grey relational analysis methodology. The optimal solution is estimated using the subsequent steps:

1st Step

The normalization is executed for output data to ensure invariable data set. In this process, output data are set in between 0 to 1. The reason for this practice is to convert the initial data to an equivalent data set. For the normalization, the greater the better logic is applied for both outputs. The process of normalization of output data is called grey relational generation. Eq. 26 is employed to evaluate the normalized value for both outputs.

$$U_k(y) = \frac{V_k(y) - \min V_k(y)}{\max V_k(y) - \min V_k(y)} \tag{26}$$

Where, U_k indicates the normalized data for k^{th} test. 'V_k' is the response data for kth test. 'k' denotes serial number of tests i.e. k= 1, 2, 3, 4,….., and 16. 'y' indicates the number of output i.e. y = 1, and 2. 'min V_k(y)' symbolize as a lowest value of 'V_k(y)' for yth output whereas 'max V_k(y)' presents the highest value of 'V_k(y)' for the yth output.

2nd Step

In this step, grey relational coefficient (GRC) σ_k is evaluated from the normalized data using Eq. 27.

$$\sigma_k(y) = \frac{\beta_{\min} + \phi\beta_{\max}}{\beta_{0k}(y) - \phi\beta_{\max}} \tag{27}$$

Where, $\beta_{0k} = \left\|U_0(y) - U_k(y)\right\|$ indicates an absolute difference between the term β_0 (y) and β_k (y). β_{max} and β_{min} are the maximum and minimum value of β_{0k}(y) congruently. ϕ is a distinctive coefficient that may varies from 0 to 1. In this research, ϕ = 0.5 is taken.

3rd Step

In this step, Grey relational grade (GRG) is calculated based on Eq. 28.

$$\lambda_k = \frac{1}{r}\sum_{y=1}^{r}\sigma_k(y) \tag{28}$$

where, λ_k is the grey relational grade for k^{th} test, r represents the number of outputs and σ_k is GRC value for k^{th} test. Now, obtained GRG value indicates the single output.

3. RESULT ANALYSIS

3.1 Model validation

The model thus developed is validated with the results of Christensen and Tonder [5]. For this purpose, the case is set to a finite journal bearing (β=1) with roughness (*Y=0.2*). Fig. 4 shows the comparison of load between the current analysis and that of Christensen and Tonder [5]. It is done for eccentricities ∈(0.1,0.3,0.5,0.6,0.7,0.8). Except the highest eccentricities ∈=0.8, the difference is less than 1% in all cases and in extreme case it is near to 2%.

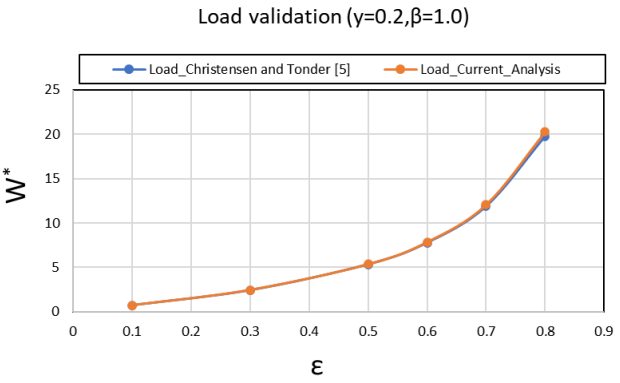

Fig. 4. Validation of load carrying capacity.

Fig. 5 shows the comparison of friction with Christensen and Tonder [5]. With same value of β, *Y* and ∈. Such validation of friction shows the difference is between (5-12) %. Such validation is encouraging, with this limitation we proceed to analyze the result of this model.

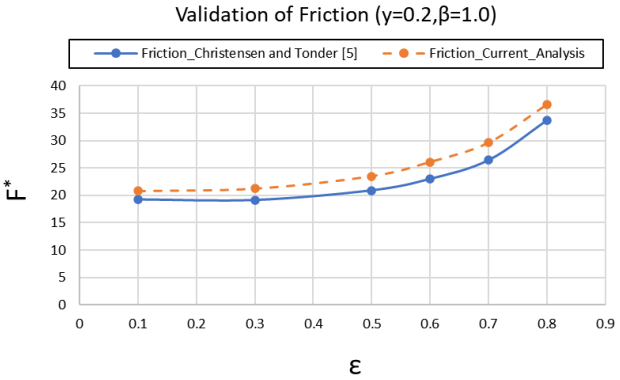

Fig. 5. Validation of friction force.

3.2 Numerical result analysis

Film thickness is one of the important parameters in bearing characteristics study. It decides the nature of lubrication (hydrodynamic / mixed / boundary). Fig. 6 shows the circumferential film profile of circular (G=0) and elliptic bore (G=0.5,0.8,1.0, 2.0 and 3.0) journal bearing. It is understood from the film that circular geometry contains one converging-diverging zone, whereas there are two such conjunctions in elliptic case. The minimum film thickness is (0.7-1.6) times radial clearance (c). The film thickness for (G=3.0) has more distinguished conjunction features.

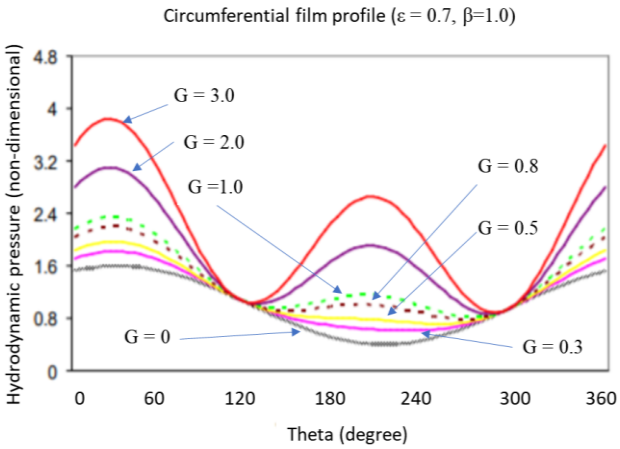

Fig. 6. Film thickness of circular and elliptic bore bearing.

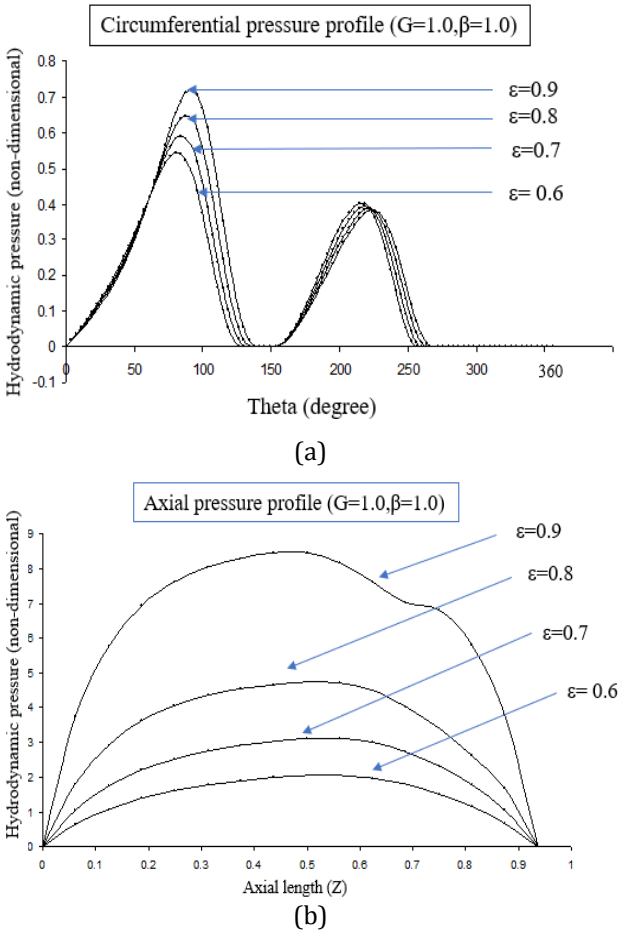

Fig. 7. (a) Circumferential pressure profile, (b) Axial pressure profile.

Fig. 7 (a) and 7 (b) shows the circumferential and axial pressure profile for (G=1.0, β=1.0) at different eccentricities ∈(0.6,0.7,0.8,0.9). Highest hydrodynamic pressure at ∈=0.9 is 35% more than that at ∈=0.6.

Fig. 8 (a) shows the variation of load ratio (G_i/G_0) with eccentricities. Elliptic bore with (G=0.5) develops load carrying capacities better than circular bore in all eccentricities, which is 1.2 to 1.4 times the former case. Elliptic bore with (G=1.0) is better that circular bore in terms load carrying capacity up to ∈=0.6. Further elliptic bore with (G=2.0,3.0) are better than circular bore upon till ∈=0.45 and 0.35 respectively. Hence on basis of load carrying capacity non-circularity up to (G=1.0) is acceptable.

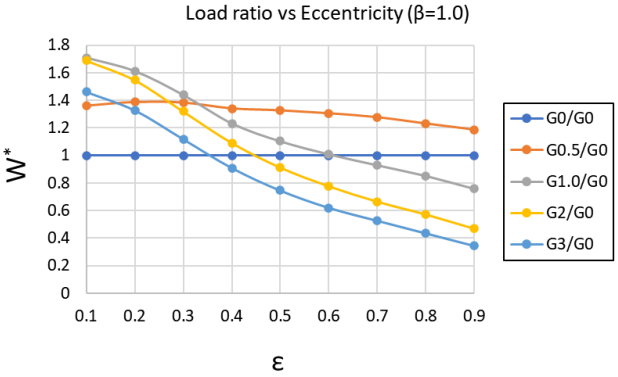

(a)

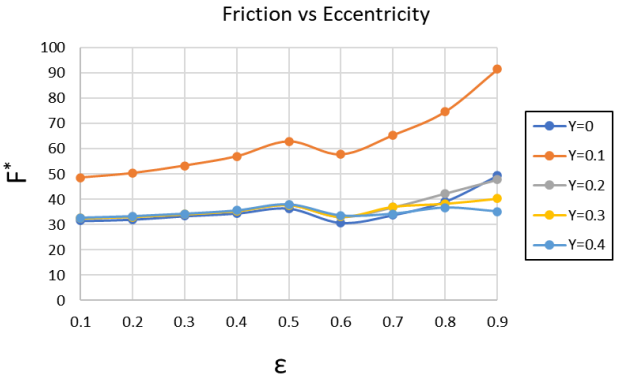

(b)

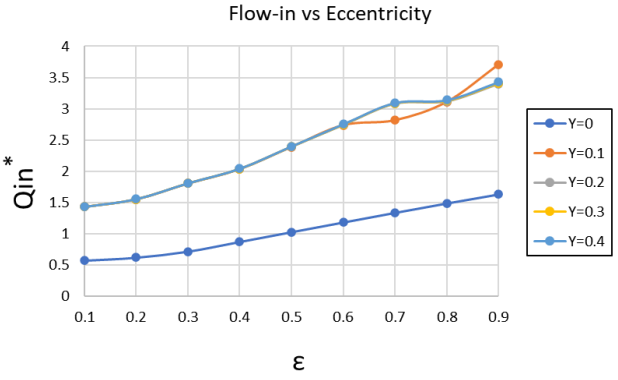

(c)

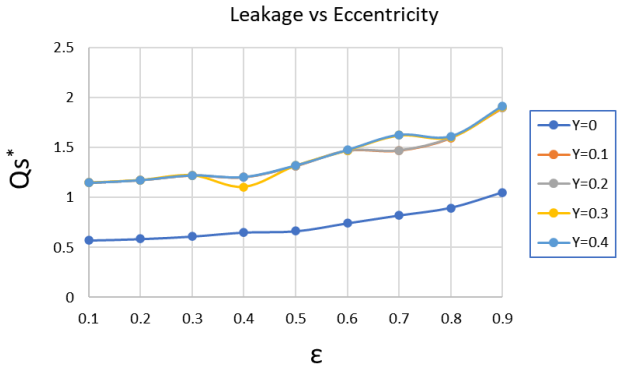

(d)

Fig. 8. (a-d) Result analysis of key performance parameters.

Fig. 8 (b) shows the variation of friction force with eccentricities for various values of roughness parameter (*Y=0.1,0.2,0.3,0.4*). Friction increases with increasing value of eccentricities for all range of roughness. But rate of change of friction (dF/d∈) is more in range of (0.6<∈<0.9). Friction is highest for (*Y=0.1*) and ranges (50-92) in (0.1<∈<0.4). Fig. 8(c) shows the variation of flow-in to the conjunction with ∈. Rough texture allows more lubricant into the conjunction compared to smooth interface. Flow-in is highest among all roughness cases at ∈=0.7 with value 3.2. Further at ∈=0.9 and roughness of (*Y=0.1*), the flow-in is 3.6. Fig. 8(d) shows the variation of side leakage with eccentricities. All rough bearings show almost two times more side leakage than smooth interface.

3.3 Optimization and confirmation test

By following three steps (Eqs 20-22), GRG data were computed and presented in Table 3, 4 and 5 respectively. The mean GRG for every input is evaluated which is given in Table 6. The optimal set of input parameters is noticed as ε2-G1-β2-Y1 Also, the rank of input terms is evaluated based on difference value of largest and smallest mean GRG data for each input. For this analysis, β is the most influencing attributes trailed by *ε*, *G* and *Y*.

Table 3. Optimization terms and their levels.

Terms	1st Level	2nd Level
Eccentricity ratio (ε)	(ε1=0.5)	(ε2=0.6)
Ellipticity (*G*)	(*G1=0.5*)	(*G2=1.0*)
L/D ratio (β)	(β1=0.5)	(β2= 1.0)
Roughness coefficient (*Y*)	(*Y1=.01*)	(*Y2=0.2*)

Table 4. Obtained results.

Test No.	ε	G	β	Y	Output-1 (W_s)	Output-2 (W_r)
1	0.5	0.5	0.5	0.1	6.3275	1.5080
2	0.5	0.5	0.5	0.2	6.5241	1.5080
3	0.5	0.5	1.0	0.1	9.2881	3.5550
4	0.5	0.5	1.0	0.2	9.1728	3.5550
5	0.5	1.0	0.5	0.1	5.6321	1.7324
6	0.5	1.0	0.5	0.2	5.5731	1.7324
7	0.5	1.0	1.0	0.1	7.5557	3.8646
8	0.5	1.0	1.0	0.2	7.4837	3.8646
9	0.6	0.5	0.5	0.1	8.7531	1.6900
10	0.6	0.5	0.5	0.2	8.6018	1.6900
11	0.6	0.5	1.0	0.1	11.9963	4.0100
12	0.6	0.5	1.0	0.2	11.8035	4.0100
13	0.6	1.0	0.5	0.1	7.0884	1.8092
14	0.6	1.0	0.5	0.2	6.9932	1.8092
15	0.6	1.0	1.0	0.1	9.3407	4.0250
16	0.6	1.0	1.0	0.2	9.2285	4.0250

Table 5. Calculated GRG results.

Test No.	Grey relational generation		GRC		GRG	Rank
	W_s	W_r	W_s	W_r		
1	0.117	0.000	0.362	0.333	0.347	14
2	0.148	0.000	0.370	0.333	0.352	13
3	0.578	0.813	0.543	0.728	0.635	7
4	0.560	0.813	0.532	0.728	0.630	8
5	0.009	0.089	0.335	0.354	0.345	15
6	0.000	0.089	0.333	0.354	0.344	16
7	0.309	0.936	0.420	0.887	0.653	5
8	0.297	0.936	0.416	0.887	0.651	6
9	0.495	0.072	0.498	0.350	0.424	9
10	0.472	0.072	0.486	0.350	0.418	10
11	1.000	0.994	1.000	0.988	0.994	1
12	0.970	0.994	0.943	0.988	0.966	2
13	0.236	0.120	0.396	0.362	0.379	11
14	0.221	0.120	0.391	0.362	0.377	12
15	0.587	1.000	0.547	1.000	0.774	3
16	0.569	1.000	0.537	1.000	0.769	4

3.4 Validation test

The validation test is accomplished with the optimal parameters. The result of Test no. 11 indicates the optimal solutions for existing data set. In validation test, predicted value of GRG is calculated at optimal parameters with use of Eq. 29.

$$\vec{\delta}=\delta_l+\sum_{k=1}^{0}\left[\delta_k-\delta_l\right] \quad (29)$$

Where, δ_l symbolizes the average value of GRG, o denotes input parameter numbers, δ_k is the greatest value of mean GRG for the individual input. The preliminary input setting is selected as the results achieved in 1st test. The validation test (Table 6) revealed a considerable growth in GRG (196.57 %) at optimal setting from the preliminary input setting GRG. This significant growth in GRG at optimal setting confirmed that the obtained optimal settings are appropriate and effective for journal bearing problem.

Table 6. Validation test results for medium ε.

Outputs	Preliminary settings ε_1-G_1-β_1-Y_1	Predicted settings ε_2-G_1-β_2-Y_1	Optimal settings ε_2-G_1-β_2-Y_1
W_s	5.8175		12.0063
W_r	1.5080		3.98
GRG	0.3385	0.8530	1.0041
Growth in GRG	0.6656		

4. CONCLUSIONS

In the current analysis, short, finite and long journal bearing are analyzed with bore ellipticities and isotropic surface roughness. Results draw some limitation of non-circularity and roughness for bearing operation. Some important outcomes are listed as below:

- Non-circularity up to (G=1.0) is better for bearing performance.
- Bearing surface with roughness parameter (*Y=0.1*) offers highest friction compared to smooth and other rough surface.
- For long journal bearing (β=2.0), non-dimensional load is highest (31.12) at $\in$=0.8.
- Highest non-dimensional friction is 45.19, which occurs for long journal bearing at (G=1.0 and $\in$=0.8).
- Highest flow-in is 6.42, which occurs at $\in$=0.8 for all short, finite and long journal bearing at G=1.0.

Limitation of current analysis is, it ignores combined cavitation effect, thermal and elastic response (Especially during higher eccentric running) which are bound to occur in high-speed rotational cases, where journal bearings are used. The present research explored the load bearing ability of journal bearing, which signifies as a key operational term for bearing contact

and material selection. The collective consequence of ε-G-β-Y on load is very complicated; therefore, optimization is executed to get the optimal solution. The obtained optimal solution ε2-G1-β2-Y1 is promising for load which is satisfactory at greater value. Moreover, roughness up to 0.1 micron is acceptable for elevated hydrodynamic pressure and improved load bearing ability. But higher order roughness (0.2, 0.3, 0.4) lessens performance, therefore not desirable in rough bearing. The future of this research work is to extend the multi-objective optimization technique for thermo elastohydrodynamics of rough and non-circular bearing. Also, to develop suitable experimental facility to validate the output of simulation and optimization.

REFERENCES

[1] J. Boyd, A. Raimondi, *Applying bearing theory to the analysis and design of journal bearing – I*, Journal of applied mechanics, vol. 18, iss. 13, pp. 298-309, 1951, doi: 10.1115/1.4010338

[2] O. Pinkus, *Solution of Reynolds equation for arbitrarily loaded journal bearings*, Journal of Fluids Engineering, vol. 83, iss 2, pp. 145-152, 1961, doi: 10.1115/1.3658905

[3] B.R. Reason, I.P. Narang, *Rapid design and performance evaluation of steady state journal bearing - A Technique amendable to programmable hand calculators*, Transaction of the ASLE, vol. 25, iss. 4, pp. 429-444, 1982, doi: 10.1080/05698198208983111

[4] W.A. Crosby, *An investigation of performance of journal bearings with slightly irregular bore*, Tribology International, vol. 25, iss. 3, pp. 199-204, 1992, doi: 10.1016/0301-679X(92)90049-S

[5] H. Christensen, K. Tonder, *The hydrodynamic lubrication of rough journal bearings*, Journal of Tribology, vol. 95, iss. 2, pp. 166-172, 1973, doi: 10.1115/1.3451759

[6] H. Christensen, *Stochastic models for hydrodynamic lubrication of rough surfaces*, Proceedings of the Institution of Mechanical Engineers, vol. 184, iss. 1, pp. 1013-1025, 1969, doi: 10.1243/PIME_PROC_1969_184_074_02

[7] D. Zhu, Y.-Z Ho, *Effect of rough surface topography and orientation on the characteristics of EHD and mixed lubrication in circular and elliptical contacts*, Tribology Transactions, vol. 44, iss. 3, pp. 391-398, 2001, doi: 10.1080/10402000108982472

[8] F. Rahmani, R.K. Pandey, J.K. Dutta, *Influence of Elliptic Bore and non-Newtonian Rheology of Lubricant on the Performance and Stability of Journal Bearing*, Procedia Technology, vol. 23, pp. 28-35, 2016, doi: 10.1016/j.protcy.2016.03.069

[9] P.C. Mishra, *Mathematical modeling of stability in rough elliptic bore misaligned journal bearing considering thermal and non-Newtonian effects*, Applied Mathematical Modelling, vol. 37, iss. 8, pp. 5896–5912, 2013, doi: 10.1016/j.apm.2012.11.020

[10] R. Turaga, A.S. Sekhar, B.C. Majumdar, *The effect of roughness parameter on the performance of hydrodynamic journal bearings with rough surfaces*, Tribology International, vol. 32, iss. 5, pp. 231-236, 1999, doi: 10.1016/S0301-679X(99)00035-3

[11] P. Liang, C. Lu, W. Pan, S. Li, *A new method for calculating the static performance of hydrostatic journal bearing*, Tribology International, vol. 77, pp. 72–77, 2014, doi: 10.1016/j.triboint.2014.04.019

[12] K.G. Binu, K. Yathish, R. Mallya, B.S. Shenoy, D.S. Rao, R. Pai, *Experimental study of hydrodynamic pressure distribution in oil lubricated two-axial groove journal bearing*, Materials Today: Proceedings, vol. 2, iss. 4-5, pp. 3453 – 3462, 2015, doi: 10.1016/j.matpr.2015.07.321

[13] S.K. Guha, *Analysis of steady state characteristics of misaligned hydrodynamic journal bearing with isotropic roughness*, Tribology International, vol. 33, iss. 1, pp. 1-12, 2000, doi: 10.1016/S0301-679X(00)00005-0

[14] F. Rahmani, J.K. Dutta, R.K. Pandey, *Performance behavior of elliptical-bore journal bearings lubricated with solid granular particulate*, Particology, vol. 27, pp. 51–60, 2016, doi: 10.1016/j.partic.2015.12.009

[15] L. Lunde, K. Tonder, *Numerical Simulation of the Effects of three-Dimensional roughness on Hydrodynamic Lubrication: Correlation coefficients*, Journal of Tribology, vol. 119, iss. 2, pp. 315-322, 1997, doi: 10.1115/1.2833216

[16] R. Turga, A.S. Sekhar, B.C. Majumdar, *The effect of roughness parameter on the performance of hydrodynamic journal bearings with rough surfaces*, Tribology International, Vol. 32, pp. 231-236, 1999, doi: 10.1016/S0301-679X(99)00035-3

[17] C. Zhang, J. Wei, F. Wang, S. Hou, A. Zhang, T.C. Lim, *Dynamic model and load sharing performance of planetary gear system with journal bearing*, Mechanism and Machine Theory, vol. 151, Available online, 2020, doi: 10.1016/j.mechmachtheory.2020.103898

[18] H. Jamali, A. Al-Hammod, *A New Method for the Analysis of Misaligned Journal Bearing*, Tribology in Industry, vol. 40, no. 2, pp. 213-224, 2018, doi: 10.24874/ti.2018.40.02.05

[19] K.A. Kokkinidis, P.G. Nikolakopoulos, *Simulation of misaligned journal bearing using Neural Network,* Tribology in Industry, Article in press, 2022, doi: 10.24874/ti.1078.03.21.10

[20] H. Jamali, A. Al-Hammod, *Effect of Cavitation on the Performance of Journal Bearings Lubricated with Non-Newtonian Lubricant*, Tribology in Industry, vol. 42, no. 4, pp. 666-678, 2020, doi: 10.24874/ti.959.09.20.11

[21] M. Kouider, Z. Djallel, Y. Abdelkader, K. Sahraoui, *Mathematical Modelling of Journal Bearing Lubricated with Non-Newtonian Fluid*, Tribology in Industry, vol. 43, no. 4, pp. 615-623, 2021, doi: 10.24874/ti.1117.05.21.09

[22] W. Hsin-Hung, *A Comparative Study of Using Grey Relational Analysis in Multiple Attribute Decision Making Problems*, Quality Engineering, vol. 15, iss. 2, pp. 209-217, doi: 10.1081/QEN-120015853

[23] P.A. Sylajakumari, R. Ramakrishnasamy, G. Palaniappan, *Taguchi Grey Relational Analysis for Multi-Response Optimization of Wear in Co-Continuous Composite*, Materials, vol. 11, iss. 9, 2018, pp. 1-17, doi: 10.3390/ma11091743

[24] R. Kumar, A.K. Sahoo, P.C. Mishra, R.K. Das, *Investigation on Tool Wear and Surface Characteristics in Hard Turning Under Air-Water Jet Spray Impingement Cooling Environment*, Tribology in Industry, vol. 41, no. 2, pp. 172-187, 2019, doi: 10.24874/ti.2019.41.02.04

[25] R. Kumar R, A.K. Sahoo, P.C. Mishra, R.K. Das, *Comparative study on machinability improvement in hard turning using coated and uncoated carbide inserts: part II modelling, multi-response optimization, tool life, and economic aspects*, Advances in Manufacturing, vol. 6, pp. 155-175, 2018, doi: 10.1007/s40436-018-0214-0

[26] A. Gupta, P.C. Mishra, *Optimization of emission characteristics of spark ignition engine with chambered straight muffler running in methanol blend: An engine development technique for environmental sustainability*, Journal of Cleaner Production, vol. 238, Available online, 2019, doi: 10.1016/j.jclepro.2019.117778

[27] S. Avikal, K.C. Nithin Kumar, A. Raj Singh, R. Jain, *Grey based Taguchi optimization for multi-lobe bearing*, Materials Today: Proceedings, vol. 26, pp. 2663-2666, 2020, doi: 10.1016/j.matpr.2020.02.560

[28] D. Dowson, G.R. Higginson, *A numerical solution to the elasto-hydrodynamic problem*, Journal of Mechanical Engineering Science, vol. 10, iss. 1, pp. 6-15, 1959, doi: 10.1243/JMES_JOUR_1959_001_004_02